Observation of bright spatial photorefractive solitons in a planar strontium barium niobate waveguide

D. Kip and M. Wesner

Fachbereich Physik, Universität Osnabrück, D-49069 Osnabrück, Germany

V. Shandarov

State University of Control Systems and Radioelectronics, Tomsk 634050, Russia

P. Moretti

Laboratoire de Physico-Chimie des Matériaux Luminescents, Université Claude Bernard, Lyon 1, 69622 Villeurbanne, France

Received February 20, 1998

We have obtained stationary bright spatial solitons in a planar photorefractive strontium barium niobate waveguide for visible light ranging from 514.5 to 780 nm. Even for larger wavelengths ($\lambda = 1047$ nm) strong self-focusing of the beam was observed; however, input power had to be some orders of magnitude higher than for visible light for self-focusing to occur. Furthermore, we found transient self-trapping of red light ($\lambda = 632.8$ nm) that corresponds to the formation of bright quasi-steady-state solitons. © 1998 Optical Society of America

OCIS codes: 060.5530, 090.2890, 060.1810, 130.0130, 190.5330.

Dark and bright spatial solitons in photorefractive materials have attracted significant interest in the past few years. First, quasi-steady-state solitons that are transient in time evolution were predicted and studied in photorefractive crystals with an externally applied electric field.[1,2] Next, the existence of dark and bright steady-state photovoltaic solitons in materials subjected to the photovoltaic effect was demonstrated.[3] Finally, in photorefractive crystals that were also biased with an external electric field, steady-state spatial solitons resulting from a nonuniform screening of this external field were obtained.[4,5] It was experimentally confirmed that photorefractive two-dimensional spatial solitons can exist at optical powers of a few microwatts,[6] which is much less than for Kerr-type solitons.[7] The low power level promises potential applications as photonic elements, e.g., all-optical switches, modulators, and beam deflectors.[8,9] For some of these applications elements in waveguide configuration may be preferrable, as they are compatible with semiconductor lasers and optical fiber technology and allow for the control of local material properties by suitable surface-doping processes.[10,11]

For most of the recent investigations of photorefractive spatial solitons of which we are aware bulk strontium barium niobate (SBN) crystals were used. Planar waveguides in SBN were shown to exhibit interesting photorefractive properties.[12] Furthermore, they can be used for nonlinear light propagation[13] and all-optical switching[14] by use of the thermo-optic and pyroelectric properties of the material. In this Letter we report what is to our knowledge the first observation of bright photorefractive solitons in waveguides.

In our experiments we used a congruently melting SBN crystal with a concentration of 0.1-wt. % CeO_2 in the melt. The dimensions of the sample were 2.0 mm × 6.0 mm × 3.3 mm, with the 3.3-mm edges along the c axis of the crystal. On both faces normal to the c axis, electrodes were prepared with silver paste. The propagation length was 6.0 mm. Implantation of the crystal with He^+ ions at an energy of 2.0 MeV and a dose of 1×10^{15} cm^{-2} yielded a buried damaged layer of reduced refractive index, $\Delta n_e \approx -0.008$, that formed a single-mode waveguide for red light ($\lambda = 632.8$ nm) with a thickness of 4.5 μm. Details of the fabrication process are described in Ref. 15.

The experimental setup is shown in Fig. 1. Beams from an Ar-ion laser ($\lambda = 514.5$ nm), a He–Ne laser (632.8 nm), a laser diode ($\lambda = 780$ nm), or a Nd:YLF laser (1047 nm) were coupled into the waveguide by a 20× microscope lens (N.A., 0.4). We chose the light polarization to excite the extraordinary wave of the crystal; thus we used an electro-optic coefficient r_{33}, which is ~5 times higher than r_{13}. A set of two cylindrical lenses in front of the in-coupling lens forms a telescope that is used to adjust the elliptical beam profile at the input face of the sample. Throughout this Letter beam diameters are given as FWHM values. The

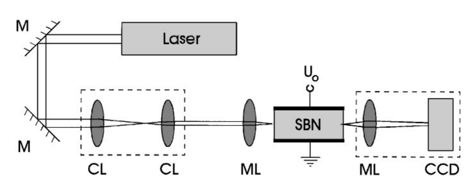

Fig. 1. Scheme of the experimental setup for spatial soliton formation in planar waveguides. M's, mirrors; CL's, cylindrical lenses; ML's, microscope lenses; U_0, externally applied high voltage; SBN, SBN waveguide.

0146-9592/98/120921-03$15.00/0

intensity distribution at the exit face of the sample was imaged by a 25× microscope lens on a calibrated CCD camera. To obtain uniform background illumination of the waveguiding layer, which is necessary for steady-state solitons, we used green light from an Ar-ion laser. The light was coupled into an optical fiber that illuminated the whole sample homogeneously from the top.

We observed the formation of bright screening solitons at light wavelengths λ of 514.5, 632.8, and 780 nm. The applied electric field E that was necessary for soliton creation ranged from ~4.5 to 10 kV/cm, depending on the initial beam diameter d_{in} and the in-coupled power P_{in}, and pointed in the direction of the positive c axis of the crystal. The background illumination in most experiments was kept at ~30 mW/cm^2. To avoid a contribution to self-focusing by thermal effects, as described in Ref. 13, we kept the input power P_{in} of the green light well below 1 mW (for longer wavelengths thermal effects can be neglected because of the low optical absorption).

In Fig. 2, we illustrate the soliton formation starting from the initially divergent He–Ne laser beam ($\lambda = 632.8$ nm) as a function of the externally applied electric field. For this case, the initial beam diameter is $d_{\mathrm{in}} \approx 10$ μm, and without an electric field it increases because of diffraction to $d \approx 130$ μm at the exit face. Because of the absorption of the guided red beam ($\alpha_e = 1.7$ cm^{-1}) the intensity ratio of the guided light to the background intensity increases by a factor of 3 when the red beam propagates toward the exit face of the sample. For electric fields smaller than 5 kV/cm, only small self-focusing is observed. However, for larger applied electric fields the dependence $d(E)$ shows a thresholdlike behavior corresponding to the formation of a light-induced waveguide channel that traps the initial light beam. Above this threshold, the beam diameter changes only slightly with electric field; this behavior is different from that of one-dimensional screening solitons in bulk. The corresponding intensity profiles $I(z)$ at the exit face of the waveguide are given in Fig. 3 for different electric fields E and an input power of $P_{\mathrm{in}} = 4.3$ μW.

When we increase the initial beam diameter to ~20 μm, the threshold value of the electric field for the formation of solitons (see Fig. 2) shifts to lower values of E. First of all, above this threshold the diameter of the solitons does not change significantly, but for even higher electric fields of 8 to 10 kV/cm we observe an increase of the beam diameter at the exit face that is followed by a splitting of the soliton into two intensity peaks; i.e., the soliton becomes unstable when the nonlinearities are too high. However, it is not yet clear why the soliton can be preserved for such a wide range of biasing electric-field values before it becomes unstable.

As in the bulk SBN crystal,[16] the self-trapping of the beam is accompanied by a strong bending of the soliton's path because of the nonlocal contribution to the refractive-index change by the photorefractive effect. In the experiment depicted in Fig. 2 and for $P_{\mathrm{in}} = 4.3$ μW, the light spot moves ~60 μm on the exit face when the electric field is increased from 7.5 to 10 kV/cm.

It should be noted that at light powers as great as some tens of microwatts steady-state solitons can be achieved even without any background illumination. A possible reason may be an increased value of the dark conductivity in the waveguiding layer because of the ion-implantation process, as discussed in Refs. 12 and 15. Using data from Ref. 12, we estimate a value of $\sigma_d \approx 10^{-8}$ A/(V m) for our sample.

We also observed bright quasi-steady-state solitons in the waveguide. These transient solitons were formed during a shorter time than the buildup time of the steady-state screening solitons, and they were found for a lower biasing electric field E.[17] The diameter of the input beam was larger than that in the experiments on steady-state solitons described above, and no background illumination was necessary. To inspect the temporal dependence of the beam profiles on the exit face of the waveguide, we captured a sequence of pictures with the CCD after the input beam was switched on and in the presence of the electric field E. Figure 4 shows the time evolution of the beam diameter d for different fields E. The initial beam size on the entrance face is $d_{\mathrm{in}} = 28$ μm, corresponding to

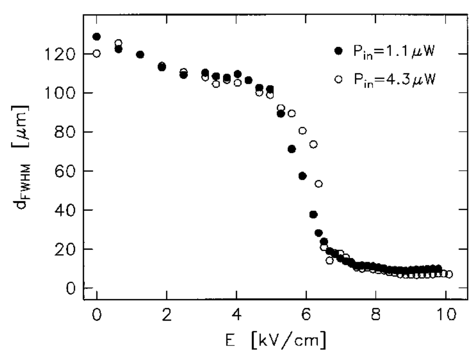

Fig. 2. Beam diameter d (FWHM) at the exit face of the waveguide as a function of the electric field E for two different input powers P_{in} of He–Ne laser light. The background illumination with green light ($\lambda = 514.5$ nm) is ~30 mW/cm^2. All diameters are measured in the steady state.

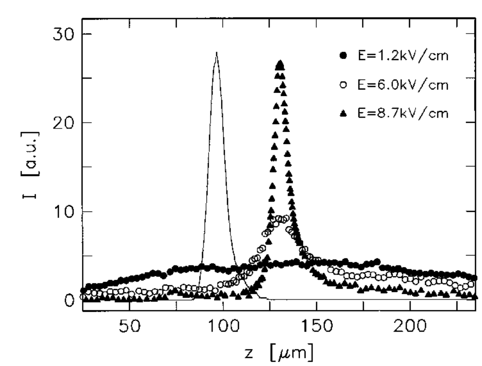

Fig. 3. Intensity profiles $I(z)$ at the exit face of the waveguide measured for different externally applied electric fields E. The profiles are for the measurement shown in Fig. 2 and an input power $P_{\mathrm{in}} = 4.3$ μW. For comparison, the solid curve shows the input beam profile (shifted for better viewing).

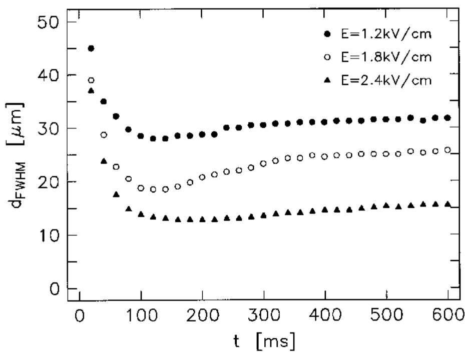

Fig. 4. Time evolution of the beam diameter d (FWHM) in the presence of different externally applied electric fields E. The input power of the He–Ne laser light is 55 μW.

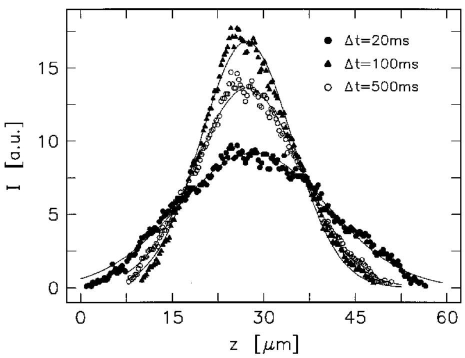

Fig. 5. Intensity profiles $I(z)$ at the exit face of the waveguide measured for different time delays Δt after the He–Ne laser beam is switched on. The profiles are for the measurement shown in Fig. 4 and $E = 1.8$ kV/cm.

a spot size $d \approx 60$ μm on the exit face. The quasi-steady-state solitons are formed within 50 to 120 ms and can be recognized by the broad minima in the dependence $d(t)$. For higher input power P_{in} the buildup time decreases further.

The temporal behavior of the beam is also illustrated in Fig. 5 for $E = 1.8$ kV/cm. The intensity profiles $I(z)$ are measured after different time delays after the light is switched on, i.e., the initial stage ($\Delta t = 20$ ms), the quasi-steady-state regime ($\Delta t = 100$ ms), and the final steady-state situation ($\Delta t = 500$ ms).

For a wavelength of $\lambda = 1047$ nm significant self-focusing of the guided light is observed. No effects can be seen for input powers of less than 0.5 mW. For an input power of ~1.3 mW (3 orders of magnitude higher than for visible light) and a high electric field of 8.5 kV/cm, strong self-focusing up to diameters of ~22 μm at the exit face occurs but without compensating completely for diffraction. This self-focusing may be due to the input diameter of the IR beam, which was ~10 μm, probably too small for soliton excitation. We plan to do further studies to test the possibility of soliton propagation at this wavelength, as this would be important for applications of spatial solitons.

In conclusion, we have obtained bright steady-state screening solitons in a planar photorefractive strontium barium niobate waveguide for visible light. In the infrared ($\lambda = 1047$ nm), strong self-focusing of the beam was observed. Furthermore, we found transient self-focusing of red light ($\lambda = 632.8$ nm) on a time scale of several tens of milliseconds that corresponds to the formation of bright quasi-steady-state solitons.

The financial support of the Deutsche Forschungsgemeinschaft (SFB 225, D9) is gratefully acknowledge.

References

1. M. Segev, B. Crosignani, A. Yariv, and B. Fischer, Phys. Rev. Lett. **68,** 923 (1992).
2. G. Duree, J. L. Schultz, G. Salamo, M. Segev, A. Yariv, B. Crosgnani, P. DiPorto, E. Sharp, and R. Neurgaonkar, Phys. Rev. Lett. **71,** 533 (1993).
3. G. C. Valley, M. Segev, B. Crosignani, A. Yariv, M. M. Fejer, and M. C. Bashaw, Phys. Rev. A **50,** R4457 (1994).
4. M. D. Iturbe-Castillo, P. A. Marquez-Aguilar, J. J. Sanchez-Mondragon, S. Stepanov, and V. Vysloukh, Appl. Phys. Lett. **64,** 408 (1994).
5. M. Segev, G. C. Valley, B. Crosignani, P. DiPorto, and A. Yariv, Phys. Rev. Lett. **73,** 3211 (1994).
6. M. F. Shih, M. Segev, G. C. Valley, G. Salamo, B. Crosignani, and P. DiPorto, Electron. Lett. **31,** 826 (1995).
7. M. Shalaby and A. J. Barthelemy, IEEE J. Quantum Electron. **28,** 2736 (1992).
8. E. D. Eugenieva, R. V. Roussev, and S. G. Dinev, J. Mod. Opt. **44,** 1127 (1997).
9. A. W. Snyder and A. P. Sheppard, Opt. Lett. **18,** 482 (1993).
10. E. Robertson, R. Eason, C. Kazmarek, P. Chandler, and X. Huang, Opt. Lett. **21,** 641 (1996).
11. S. M. Kostritskii and O. M. Kolesnikov, J. Opt. Soc. Am. B **11,** 1674 (1994).
12. D. Kip, B. Kemper, I. Nee, R. Pankrath, and P. Moretti, Appl. Phys. B **65,** 511 (1997).
13. D. Kip, E. Krätzig, V. Shandarov, and P. Moretti, Opt. Lett. **23,** 343 (1998).
14. D. Kip, M. Wesner, E. Krätzig, V. Shandarov, and P. Moretti, Appl. Phys. Lett. **72,** 1960 (1998).
15. D. Kip, S. Aulkemeyer, and P. Moretti, Opt. Lett. **20,** 1256 (1995).
16. M. F. Shih, P. Leach, M. Segev, M. H. Garret, G. Salamo, and G. C. Valley, Opt. Lett. **21,** 324 (1996).
17. M. Morin, G. Duree, G. Salamo, and M. Segev, Opt. Lett. **20,** 2066 (1995).